Journal of Ceramic Processing Research. Vol. 26, No. 2, pp. 239~247 (2025)
(Received 30 November 2024, Received in revised form 18 February 2025, Accepted 1 March 2025)
https://doi.org/10.36410/jcpr.2025.26.2.239

J O U R N A L O F
Ceramic Processing Research

Experimental Study of the novel high-efficiency SrO-CeO_2 adsorbent for cyclic CO_2 capture

Kuanyu Zhu[a], Qiuwan Shen[a,*], Xin Zhang[a], Min Yan[b] and Shian Li[a]
[a]*Marine Engineering College, Dalian Maritime University, Dalian, China*
[b]*Department of Thermal Engineering, Shandong Jianzhu University, Jinan, China*

With increasing global attention on environmental protection, reducing CO_2 emissions from shipping is urgent. This study explores post-combustion CO_2 capture using adsorbents for marine exhaust. A SrO-based CO_2 adsorbent supported by CeO_2 was prepared via sol-gel method, and its cyclic adsorption capacity was tested through fixed-bed experiments. The impact of dopants, carbonation temperature, and CO_2 concentration on adsorption performance was studied, and the microstructure was analyzed using X-ray Diffraction (XRD), Scanning Electron Microscopy (SEM), Energy Dispersive Spectroscopy (EDS), and Brunauer-Emmett-Teller (BET). Results show that Ce-2SrO demonstrates excellent performance and stability at 880 °C and 950 °C under adsorption-desorption conditions, retaining about 93% CO_2 adsorption efficiency after 20 cycles. SEM and EDS reveal that CeO_2 is evenly distributed within SrO pores, enhancing pore structure stability, adsorption capacity, and resistance to sintering. SrO-based adsorbents show excellent thermal sintering resistance due to CeO_2. Additionally, CeO_2 promotes ion migration during carbonation, helping maintain adsorption activity. This study presents a novel approach for synthesizing efficient, stable CO_2 adsorbents and offers a new strategy for marine carbon capture.

Keywords: CO_2 capture, Adsorbent, Ce-2SrO, High efficiency, Cyclic stability.

Introduction

Given the exponential increase in global population and energy usage, the issue of global climate change has escalated significantly, with CO_2 emissions becoming a major global concern. Currently, CO_2 generated from the using of fossil fuels and cement production constitutes 87% of all CO_2 emissions from human activities, and the majority of marine transportation still relies on fossil fuels for power. The technology of CCUS (CO_2 capture, utilization, and storage) is acknowledged as one of the most economically efficient strategies to swiftly reduce CO_2 emissions due to its technical attributes [1-3]. CO_2 capture technology forms a crucial component of CCUS technology. In addition to the benefits of conventional CCUS, it also offers the advantages of straightforward operation, cost-effectiveness, and high efficiency [4-6]. CO_2 capture can be categorized into three types: pre-combustion, oxygen-enriched, and post-combustion capture. Currently, post-combustion capture is extensively employed in power plants and stands as the most advanced method of carbon capture to date [7]. Figure 1 shows the process flow of post-combustion CO_2 capture for marine. Marine vessels can easily adapt their existing exhaust gas treatment systems without altering the engine or the entire system, and the capital investment is minimal. Therefore, it is the most probable method to be implemented for capturing CO_2 from marine exhaust.

Undoubtedly, the efficiency and stability of adsorbents are fundamental to CO_2 capture. Adsorbents can be classified into low-temperature, medium-temperature, and high-temperature categories based on their carbonation temperature. Presently, MgO and CaO are the most researched adsorbents, falling under the medium and high-temperature categories respectively. CaO-based adsorbents, with their high theoretical adsorption capacity, abundant availability, and cost-effectiveness, are regarded as superior high-temperature CO_2 adsorbents [8]. However, under high-temperature reaction conditions, the reactivity of calcined regenerated CaO decays rapidly due to sintering [9]. Therefore, many studies have been devoted to improving the structure of adsorbents to improve their CO_2 capture ability, including chemical pretreatment, preparation methods, and precursor composition [10]. On the contrary, doping heat-resistant metal oxides can effectively reduce the sintering phenomenon of adsorbents, such as Al_2O_3, Y_2O_3, SiO_2, TiO_2, ZrO_2, MgO, and CeO_2, which are widely studied [11]. Wu proposed a synchronous titration-calcination method to synthesize a CaO-based adsorbent with CeO_2 as support. It was determined that optimal CO_2 adsorption performance is achieved when the doping ratio of Ca to Ce is 24:1, and the adsorption capacity remained high after 15 cycles [12]. At present,

*Corresponding author:
Tel : +86-18624118015
Fax: +0411-84728659
E-mail: shenqiuwan@dlmu.edu.cn

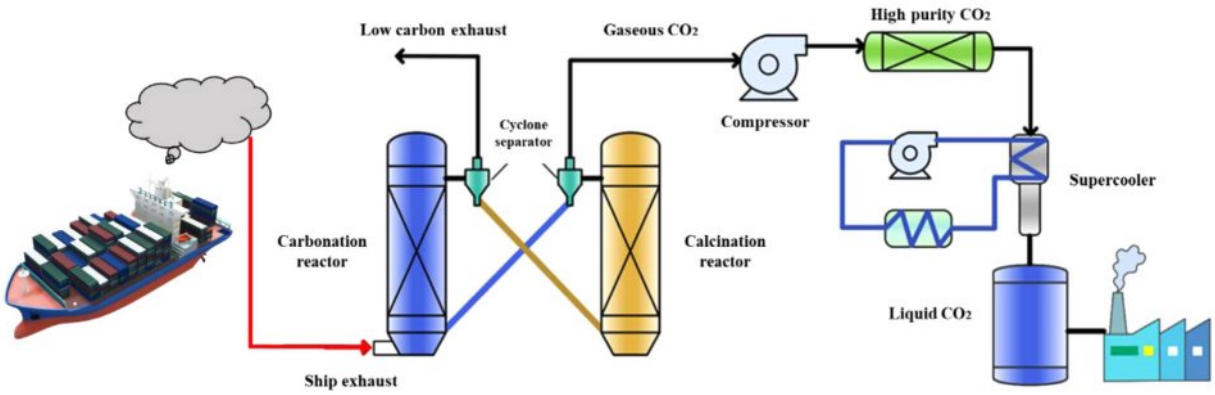

Fig. 1. Flow chart of post-combustion CO_2 capture for marine exhaust.

the support of SrO is also being studied. Gigantino synthesized a SrO-based adsorbent with MgO as a dopant and tested its cycle stability [13]. It is concluded that MgO doping can alleviate the deactivation caused by the sintering of the adsorbent. Andr'e also used MgO as a sintering inhibitor and stabilizer of SrO, and experimented in multiple cycles and different gas atmospheres, and concluded that MgO doping prevented a significant loss of adsorbent activity [14]. Despite acting as physical barriers between neighboring adsorbent particles, reducing the rate of sintering, and preserving the pore structure, the support can still function effectively, they still have the problem of reactivity decay in multiple cycles, so it is still necessary to develop highly stable CO_2 adsorbents.

Consequently, this study proposes a novel high-efficiency SrO-based adsorbent for marine CO_2 capture. CeO_2, ZrO_2, and Al_2O_3, which are widely studied supports, can facilitate the uniform distribution of SrO and mitigate the aggregation of adsorbent particles, thus delaying the sintering of adsorbents. Simultaneously, they possess a high Taman temperature to prevent the pore structure of the adsorbent from aggregating. As such, this study investigates the CO_2 capture performance of SrO supported by different supports. Furthermore, the adsorption properties of Ce-2SrO at varying carbonation temperatures and CO_2 concentrations are discussed, and the adsorption stability of Ce-2SrO is validated through cyclic adsorption experiments. These works collectively provide a reference for the application of marine CO_2 capture.

Experimental

Preparation of Adsorbent

The sol-gel method is used to prepare the Ce-2SrO adsorbent, and the preparation process is shown in Figure 2. $Sr(NO_3)_2{\cdot}4H_2O$ and $Ce(NO_3)_3{\cdot}6H_2O$ were dissolved in 100 ml of deionized water in a molar ratio of 2:1. Then citric acid and ethylene glycol were added according to the molar ratio of metal ion to complexing agent, and the molar ratio of ethylene glycol: citric

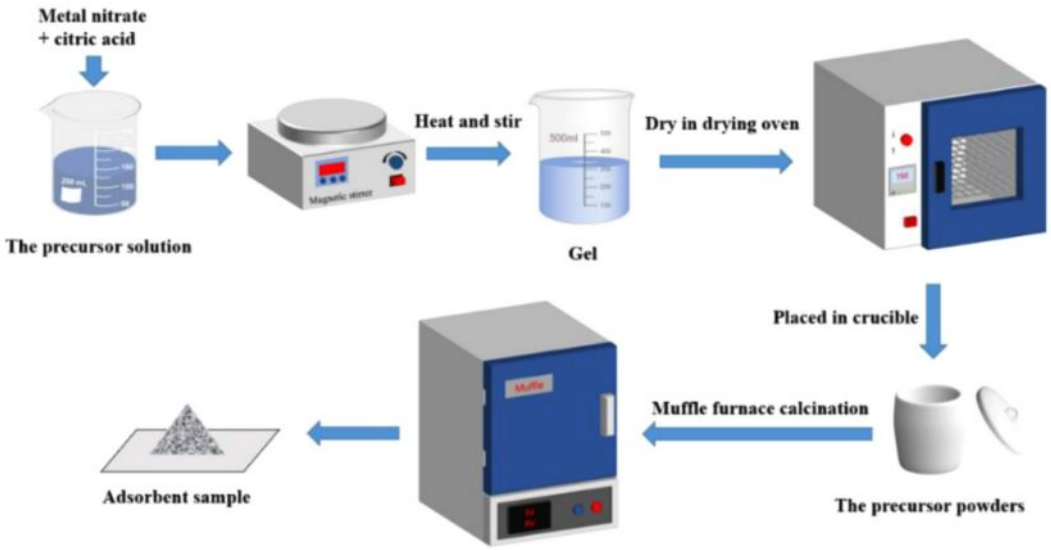

Fig. 2. Flow chart of the synthesis method.

Table 1. Overview of SrO-based sorbents prepared in the present study.

No.	Sample	Molar ratio of metal oxides/SrO
1	Ce-2SrO	2 : 1
2	Zr-2SrO	2 : 1
3	Al-2SrO	2 : 1

acid: metal ion was 3.75: 2.5: 1. After proper stirring, place the beaker in a water bath at 80 ℃ and stir for about 2 hours until a gelatinous mixture is obtained. After that, the gel was dried in a drying oven at 150 ℃ for 12 hours to obtain the xerogel. In the next step, the xerogel is completely ground and calcined in a muffle furnace at a temperature of 900 ℃ for 3 hours. Finally, the sample is taken out, cooled, and ground to obtain the adsorbent sample. The preparation process of the other two samples is similar. They are Zr-2SrO and Al-2SrO respectively.

CO_2 cyclic adsorption experiment

The experimental device for CO_2 cyclic adsorption is shown in Fig. 3. Adsorption experiment: Prior to the cyclic adsorption experiment, measure approximately 500 mg of the adsorbent sample and position it in the center of a tubular furnace, the sample was thermally treated (calcined) at 950 ℃ in 200 ml/min N_2 atmosphere for 15 min, then taken out and cooled to room temperature, weighed, and recorded. Subsequently, the sample was placed in the middle of a tubular furnace, CO_2 with a flow rate of 300 ml/min was introduced, and the sample was carbonated at 880 ℃ for 15 minutes. After carbonation is complete, the sample is cooled down to room temperature and weighed. And the material adsorbed by CO_2 was calcined in a nitrogen atmosphere at 950 ℃ for 15 minutes for regeneration. Complete the cycle experiment by repeating the aforementioned adsorption and calcination procedures.

The above carbonation/calcination process was repeated 20 times, and the adsorption efficiency of the adsorbent was calculated according to the formula:

$$\eta_s = \frac{m_s - m_d}{m_d \times A} \times \frac{M_{SrO}}{M_{CO2}} \quad (1)$$

In the formula, m_s is the actual mass (g) of the adsorbent during the reaction. m_d is the mass (g) of the adsorbent after the first calcination. A is the mass ratio of SrO in the adsorbent, M_{SrO} and M_{CO2} are the relative molecular mass of SrO and CO_2, respectively.

Characterization

An Ultima IV X-ray diffractometer, a product of Japan's Rigaku Company, was employed for the determination of the adsorbent's phase and crystal phase analysis. The sample was situated on a glass slide with a copper target inside the X-ray diffractometer. The scanning parameters were set to cover a range from 10° to 90° at a rate of 5° per minute. The collected data was then analyzed using Highscore software.

The morphology and elemental distribution of the samples were inspected using the SUPRA 55 SAPPHIRE field emission scanning electron microscope, manufactured by ZEISS Company, Germany. The imaging for Scanning Electron Microscopy (SEM) was obtained through either backscattered electron beams or secondary electrons. Prior to testing, the samples underwent a gold coating process in a vacuum for 150 seconds. The microscope was operated with an amplification factor that varied from 10 to 100 K, and an acceleration voltage that ranged between 5 and 20 kV.

The adsorption and desorption of the adsorbent were carried out using the ASAP 2460 Automatic Specific Surface Area and Porosity Analyzer, a Micromeritics product from the USA. Nitrogen was used as the analysis gas, and the bath temperature was maintained at 77.3 K. During the analysis, the pressure tolerance for both adsorption and desorption was set at 0.100, with an equilibration time of 60 seconds per stage and an equilibration timeout of 240 seconds. The adsorbents' specific surface area and pore characteristics were assessed using a multimolecular layer adsorption theory and a model for calculating pore size distribution. The total pore volume was measured at a relative pressure of P/Ps = 0.98409.

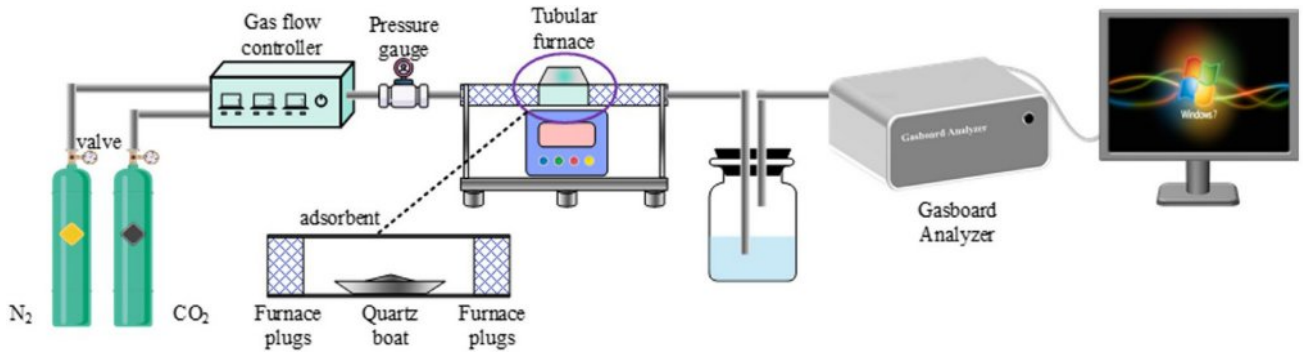

Fig. 3. Diagram of the set-up of the CO_2 cyclic adsorption experiment.

Results and Discussion

XRD Characterization

XRD was used to characterize fresh Ce-2SrO, as well as Al-2SrO, Zr-2SrO, and Ce-2SrO after primary carbonation and 20 cycles, and their crystal structures were analyzed. The XRD of Ce-2SrO at different stages is shown in Fig. 4, the characteristic peaks of SrO and CeO_2 can be clearly observed in fresh samples, corresponding to standard cards (PDF#97-067-0284) and (PDF#99-000-0623), respectively, indicating the formation of SrO and CeO_2 crystal phases. However, no diffraction peaks were observed for the composite products formed between Sr and Ce, indicating that SrO and CeO_2 were adsorbents formed through physical doping [15]. In addition, the characteristic peak containing $Sr(OH)_2(H_2O)$ was also observed, which is due to the water absorption of SrO [16]. An extremely obvious characteristic peak of $SrCO_3$ can be observed in the Ce-2SrO sample after primary carbonation, in which the characteristic peak of SrO basically does not exist, indicating that SrO in the adsorbent is completely carbonated, which indicates that the adsorbent can be effectively utilized. The characteristic peak of $SrCO_3$ is hardly visible in the Ce-2SrO sample after 20 cycles, while the characteristic peaks of SrO and CeO_2 are still clearly visible, which suggests that the introduction of CeO_2 inhibits the growth and agglomeration of SrO crystals, which is advantageous for CO_2 sequestration across numerous cycles.

Fig. 5 and Fig. 6 show the XRD patterns of Al-2SrO and Zr-2SrO after primary carbonation and 20 cycles, respectively. Although they have been desorbed at high temperatures, there are still many characteristic peaks of $SrCO_3$. And with the increase in cycle times, the number of SrO characteristic peaks is also significantly reduced, which shows that the cyclic stability of Zr-2SrO and Zr-2SrO is not satisfactory. With the increase in cycle times,

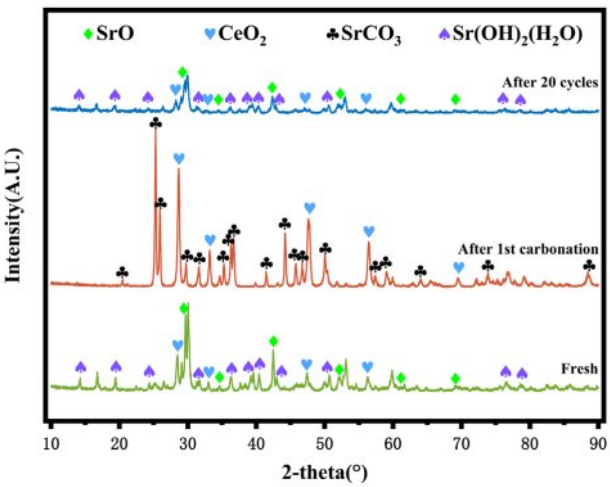

Fig. 4. XRD patterns of SrO-CeO_2 at different stages of the reaction.

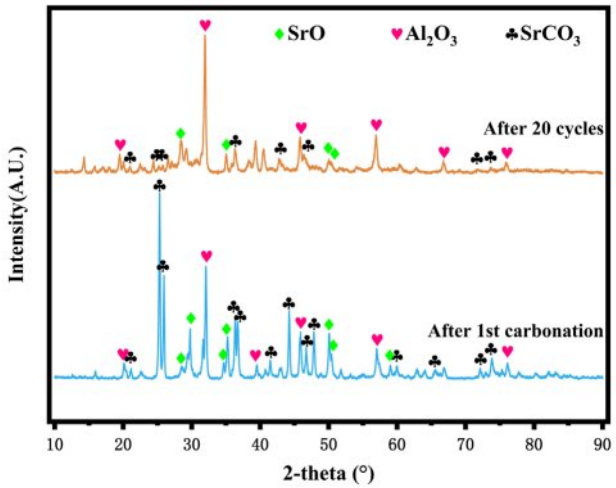

Fig. 5. XRD patterns of Al-2SrO after 1st carbonation and 20 cycles.

the adsorption efficiency of the adsorbents is weakening because of the collapse of the pore structure and sintering of the adsorbents. In addition, the characteristic peak of $SrZrO_3$ was observed in Fig. 6, which indicates that the heat resistant substance $SrZrO_3$ was produced during the synthesis of Zr-2SrO, and $SrZrO_3$ was formed by a solid-solid reaction between SrO and ZrO_2 [17].

SEM and EDS analysis

The surface morphology of the Ce-2SrO adsorbent after fresh, first carbonation, and 20 cycles was observed by scanning electron microscopy (SEM), as shown in Fig. 7. From Fig. 7a, it shows that the fresh Ce-2SrO samples have a loose and porous structure, and that many pores are uniformly distributed in the sample particles, which is helpful in realizing an efficient carbonation process. Fig. 7b shows Ce-2SrO samples after the first

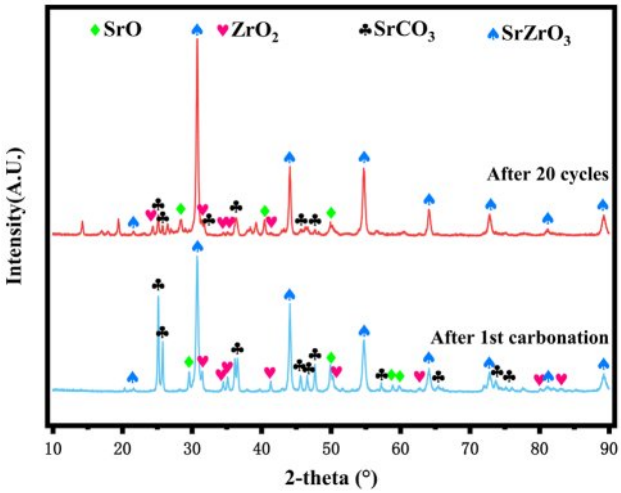

Fig. 6. XRD patterns of Zr-2SrO after 1st carbonation and 20 cycles.

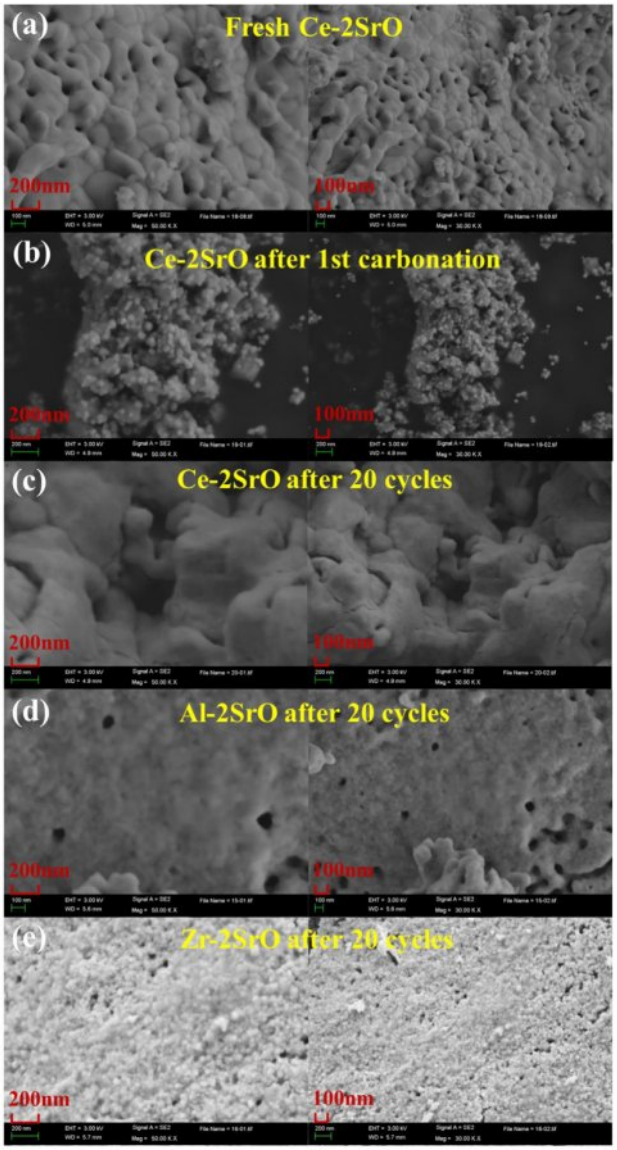

Fig. 7. (a-e) SEM images of adsorbents at different stages of the reaction.

carbonation. It is clear that many white and uniformly distributed particles appear on the surface of the samples, which may be $SrCO_3$ particles produced after SrO in the adsorbent fully absorbs CO_2. Fig. 7c shows the microstructure of Ce-2SrO after 20 cycles. It can be found that there are no impurities on the surface of the adsorbent particles, and there are still pore structures and many cracks. These pore structures and cracks can help CO_2 continue to fully contact and react with effective reactants in adsorbent [16]. Fig. 7d-e show the micromorphology of Al-2SrO and Zr-2SrO adsorbents after 20 cycles. It can be seen that Al-2SrO sintering is the more severe, and there is particle agglomeration on its surface, making it difficult for CO_2 to diffuse inside the adsorbent, which can weaken the adsorption performance of the adsorbent. In addition, after 20 cycles

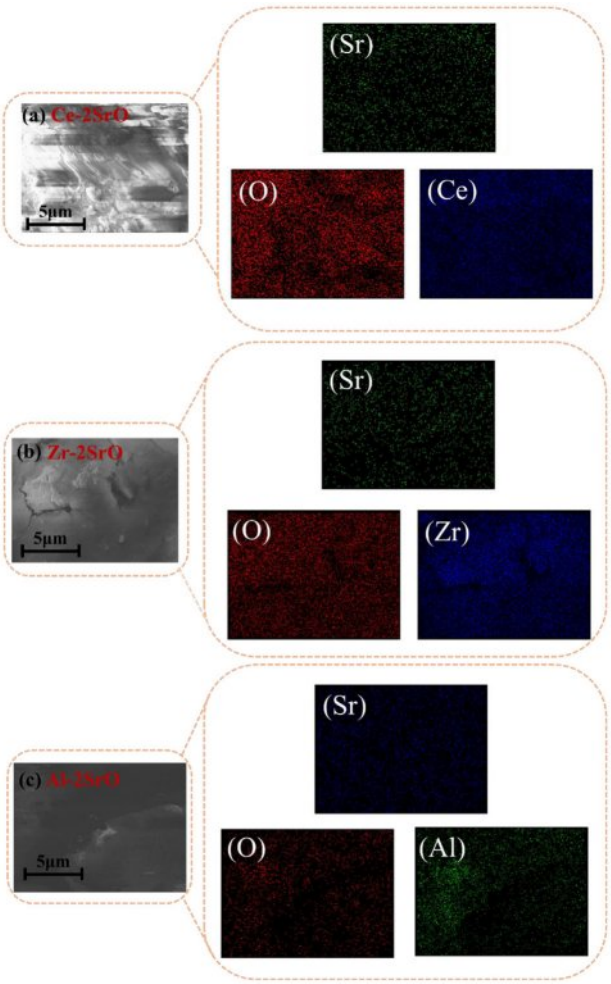

Fig. 8. (a-c) EDS-Mapping maps of adsorbents.

the microstructure of the Zr-2SrO adsorbent shows a dense surface morphology, which leads to a decrease in the adsorption capacity of Zr-2SrO adsorbent for CO_2. Ce-2SrO exhibited excellent cyclic stability compared to the other two sorbents, which corresponded to the results of XRD.

Fig. 8 shows the EDS diagrams of Ce-2SrO, Zr-2SrO, and Al-2SrO, illustrating the uniform distribution and high dispersion of elements in the adsorbent. Fig. 8a confirms the presence of Sr, Ce, and O in the adsorbent, with the distribution of these elements in Ce-2SrO aligning well with the sample selection shape. The atomic percentages of Sr and Ce are 17.76% and 7.85%, respectively, approximating a 2:1 ratio. This, alongside XRD analysis results, substantiates the successful synthesis of Ce-2SrO. Additionally, Fig. 8a reveals the uniform distribution of CeO_2 in the adsorbent, which helps prevent sintering among SrO particles. This maintenance of the pore structure bolsters the adsorbent's cyclic stability. Furthermore, the evenly dispersed SrO particles increase CO_2 active sites, enhancing the CO_2 capture capacity of the adsorbent [17].

Table 2. Specific surface area, Pore volume, and Pore size of the adsorbents.

Samples	S_{BET} ($m^2 \cdot g^{-1}$)	Pore volume ($cm^3 \cdot g^{-1}$)	Average pore size (nm)
Fresh Ce-2SrO	4.34	0.067	61.98
Fresh Al-2SrO	4.23	0.057	53.49
Fresh Zr-2SrO	5.42	0.050	36.92
Ce-2SrO after 20 cycles	2.92	0.027	157.24
Al-2SrO after 20 cycles	3.41	0.057	66.60
Zr-2SrO after 20 cycles	3.29	0.034	41.32

BET and N_2 Sorption analysis

The porous structure can enhance the adsorption capacity and gas transfer rate of CO_2 adsorbents. To further investigate the CO_2 capture capability of SrO-based adsorbents on different supports, three types of samples were characterized using the BET method. The results are displayed in Fig. 9 and Table 1. Fig. 9 presents the pore size distribution curves and N_2 adsorption-desorption isotherms of each sample. As observed in Fig. 9a, fresh Ce-2SrO exhibits a more uniform distribution of pores compared to the other two samples, with a significantly higher proportion of larger pores. The pore size distribution of Ce-2SrO after 20 cycles also shows greater uniformity and a relatively higher proportion

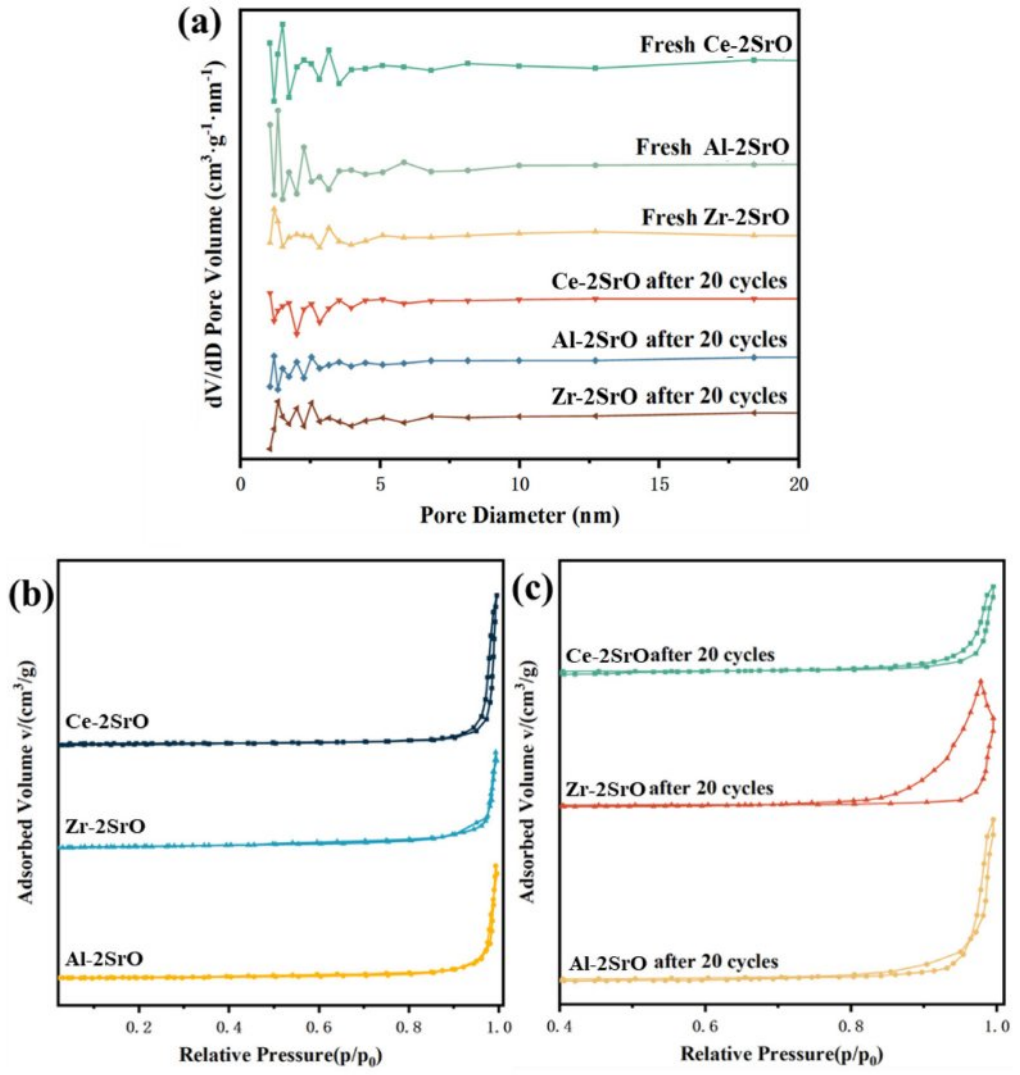

Fig. 9. (a-c) Pore size distribution and N_2 adsorption-desorption isotherms of variable adsorbents.

Table 3. Comparison of adsorption capacity and stability of Ce-2SrO and other adsorbents.

No.	Adsorbent	CO_2 uptake (mg/g)	Stability (mg/g)	Ref.
1	Ce-2SrO	239	227 (20^{th} cycle)	This study
2	Rod-like MgO	68.64	64.68 (10^{th} cycle)	[19]
3	Lamellar shaped MgO	102.96	83.6 (10^{th} cycle)	[20]
4	Foam-like MgO	114.84	92.972 (6^{th} cycle)	[21]
5	Al_2O_3-MgO	131.12	114.84 (6^{th} cycle)	[22]
6	CeO_2-MgO	35.288	23.49 (15^{th} cycle)	[23]
7	$CaCO_3$-MgO	43	32 (10^{th} cycle)	[24]

of larger pores compared to the other samples. Fig. 9b indicates that the synthesized adsorbents exhibit Type IV isotherms with H3 type hysteresis loops, suggesting the presence of mesoporous structures. The N_2 adsorption capacity of the samples increases sharply at higher relative pressures ($p/p_0 > 0.8$), and the capacity of Ce-2SrO is notably higher than that of the other adsorbents, indicating a relatively developed porous structure in this sample [18]. Table 2 shows the specific surface area, pore volume, and pore size distribution of each sample. The results demonstrate that Ce-2SrO possesses the largest pore volume and size, along with a relatively high specific surface area. After 20 cycles, the pore size of Ce-2SrO increases to 2.5 times its original size. Adequate pore size effectively prevents the filling and clogging of $SrCO_3$ during the adsorption process. This confirms the strong CO_2 capture capability of Ce-2SrO, which is consistent with the SEM observation results.

CO_2 Cyclic test analysis

The cycling stability of CO_2 adsorbents plays a crucial role in carbon cycling capture. In this part, multiple cycle experiments were conducted to compare the three types of adsorbents. The CO_2 adsorption efficiency of the sorbents with the carbonation/calculation temperature of 880 °C/950 °C is shown in Fig. 10. It can be clearly seen that Ce-2SrO has a higher adsorption efficiency than the others, and the adsorption efficiency of Ce-2SrO is as high as 97.5%, with an adsorption capacity of 233 mg/g. In addition, due to the addition of CeO_2, the adsorbent has higher cycling stability, and the adsorption efficiency can still maintain 92.3% after 20 cycles, with an adsorption capacity of 220.6 mg/g. The SrO adsorbent Zr-2SrO doped with ZrO_2 can only achieve an adsorption efficiency of 82.2% after the first cycle, and the adsorption efficiency decreases rapidly with the increase of the cycle number. However, the formation of a heat resistant material $SrZrO_3$ enhances its cyclic performance [17], and the adsorption efficiency ultimately remains around 60%-70%. Al-2SrO adsorbents doped with Al_2O_3 showed an unsatisfactory adsorption efficiency compared with the other two adsorbents, which only reached 60.4% after the first cycle, and with

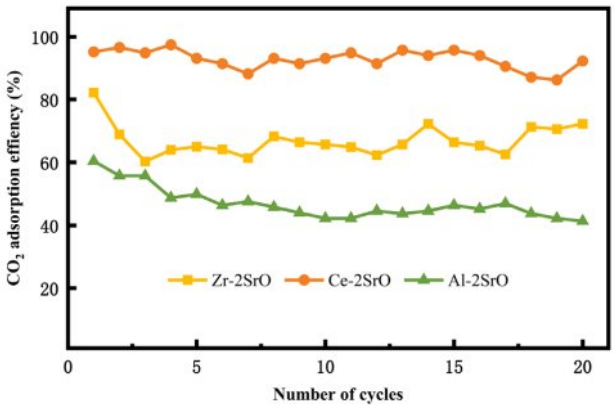

Fig. 10. CO_2 cyclic adsorption efficiency of SrO-based adsorbents on different supports with the carbonation/calculation temperature of 880 °C/950 °C.

the increase of cycle times, the adsorption efficiency slowly decreased, ultimately dropping to 41.3% after the 20th cycle. This is attributed to the decrease of adsorption efficiency caused by sintering of adsorbents at high temperature, which corresponded to the results of XRD and SEM. In addition, we compared the initial adsorption amount and the 20th cycle adsorption amount of Ce-2SrO with other adsorbents, and the summary results are shown in Table 3. The comparison results show that both the initial adsorption amount and the last cycle adsorption amount are higher than other adsorbents, and the adsorption stability is the best.

Fig. 11 shows the CO_2 cyclic adsorption efficiency of Ce-2SrO at different carbonation temperatures. As the temperature increases, the adsorption efficiency of the adsorbent also increases. With the increase in cycle numbers, the Ce-2SrO adsorbent can still maintain high adsorption efficiency as well as the stable adsorption capacity. Fig. 12 shows the CO_2 adsorption efficiency of Ce-2SrO at different CO_2 concentrations. It can be concluded that with the increasing of CO_2 concentration, the adsorption efficiency of adsorbent also increases from about 80% to about 95%. This is mainly because that at low CO_2 concentrations, the carbonation process of the adsorbent is not fully completed [25, 26]. Furthermore, as

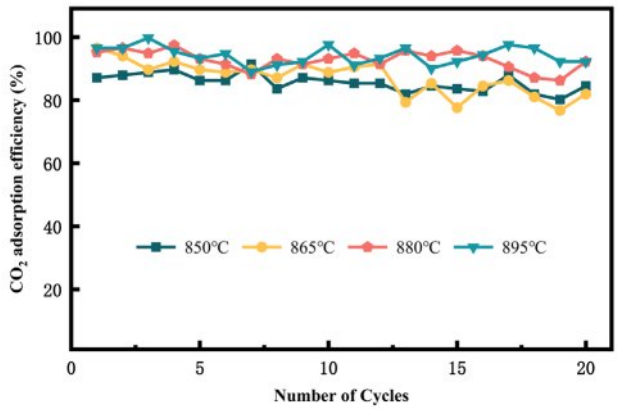

Fig. 11. CO_2 cyclic adsorption efficiency of Ce-2SrO at different carbonation temperatures.

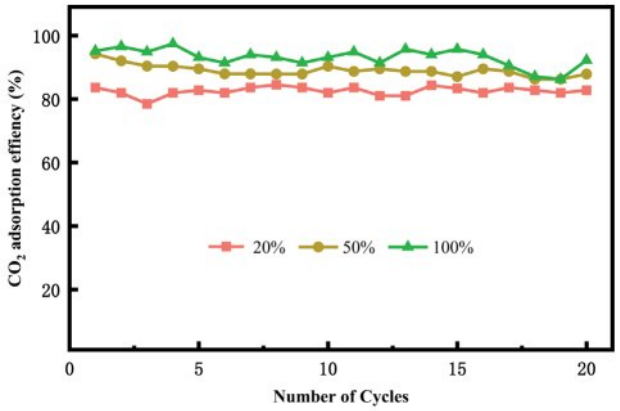

Fig. 12. CO_2 cyclic adsorption efficiency of Ce-2SrO at different CO_2 concentrations.

the number of cycles increases, the adsorption efficiency remains stable, also indicating that Ce-2SrO as a CO_2 adsorbent has excellent stability.

Conclusions

In this study, a novel high-efficiency SrO-based adsorbent has been studied that can be used as a promising adsorbent for marine CO_2 capture. The cyclic stability of the three adsorbents was tested by the CO_2 cyclic adsorption experiment. In addition, the adsorption efficiency of Ce-2SrO at different carbonation temperatures and CO_2 concentrations was also discussed. The physical and chemical properties of the adsorbent were characterized by XRD, SEM, EDS, and BET. The main conclusions can be drawn as follows.

(1) The adsorption efficiency of Ce-2SrO was nearly 100% (99.74%) at a carbonation temperature of 895 °C, reaching a theoretical adsorption capacity of 239 mg/g. In addition, the adsorption efficiency did not fluctuate obviously in 20 cycles of CO_2 adsorption experiments, and remained at about 95%. The average adsorption efficiency was 94.3% in 20 cycles. Therefore, Ce-2SrO has excellent adsorption efficiency and cyclic stability.

(2) XRD results show that SrO in Ce-2SrO adsorbent can be completely converted into $SrCO_3$ during carbonation. After 20 cycles, the characteristic peaks of the Ce-2SrO adsorbent remained the same as those of fresh samples, which indicated that the Ce-2SrO adsorbent had a high conversion rate and high cyclic stability. The results of SEM show that CeO_2 can be effectively used as a support for SrO. After 20 cycles of experiments, CeO_2 can maintain a porous structure and produce cracks to promote the full reaction between CO_2 and adsorbent. The BET results indicate that compared to the other two adsorbents, Ce-2SrO has the largest pore volume, pore size, and relatively high specific surface area, and still has the largest pore volume after 20 cycles. This can effectively demonstrate that Ce-2SrO has excellent CO_2 adsorption capacity and cycling stability.

(3) Under the experimental conditions of carbonation/calcination temperature of 880 °C/950 °C, the adsorption efficiency of CO_2 is in the order of Ce-2SrO>Zr-2SrO>Al-2SrO. The adsorbent with CeO_2 as the support can still maintain excellent adsorption efficiency and cycling stability after 20 cycles. However, Zr-2SrO and Al-2SrO cannot maintain good adsorption efficiency and cycling stability. As the number of cycles increases, the adsorbent will sinter and destroy its pore structure. In general, Ce-2SrO can be used as a novel high-performance adsorbent for CO_2 capture from marine exhaust.

Acknowledgments

This work was supported by the Science and Technology Projects of Liaoning Province (No. 2023JH1/10400077).

Conflicts of Interest

The authors declare no conflict of interest.

References

1. Y.F. Sun, Q.W. Shen, X. Zhang, G.K. Chen, K.Y. Zhu, and S.A. Li, J. Ceram. Process. Res. 25[4] (2024) 664-672.
2. S.A. Li, R.Q. Wei, Y.H. Jiang, Q.W. Shen, G.G. Yang, and N.B. Huang, J. Ceram. Process. Res. 21 (2020) 64-68.
3. X. Zhang, Q.W. Shen, K.Y. Zhu, G.K. Chen, G.G. Yang, and S.A. Li, J. Mar. Sci. Eng. 11[12] (2023) 2229.
4. G.K. Chen, Q.W. Shen, S.A. Li, X. Zhang, Z.W. Cai, and G.G. Yang, J. Sol-Gel Sci. Technol. 108[3] (2023) 721-733.
5. Q.W. Shen, Z.C. Shao, Y.H. Jiang, S.A. Li, G.G. Yang, N.B. Huang, and X.X. Pan, J. Ceram. Process. Res. 22 (2021) 576-583.
6. F. Granados-Correa, J.L. Iturbe-García, and J. Bonifacio-Martínez, J. Ceram. Process. Res. 20 (2019) 597-602.
7. N. Subramanian and P. Madejski, Energy 282 (2023) 128311.
8. J. Ding, C. Yu, and J. Lu, Appl. Energy 263 (2020) 114681.

9. R.H. Borgwardt, Chem. Eng. Technol. 44[1] (1989) 53-60.
10. C. Dang, Y. Li, and S.M. Yu, Energy Environ. Sci. 11[3] (2018) 660-668.
11. J. Chen, L. Duan, and Z. Sun, Energy Fuels 34[7] (2020) 7806-7836.
12. J. Wu, X. Liu, and R. Zhang, Chem. Eng. Technol. 454 (2003) 140485.
13. M. Gigantino, D. Kiwic, and A. Steinfeld, Solar Energy 188 (2019) 720-729.
14. L. Andr'e and S. Abanades, Energy Storage 13 (2017) 193-205.
15. A. Thirunavukkarasu and R. Nithya, J. Taiwan Inst. Chem. E. 111 (2020) 44-62.
16. H. Gu, G. Song, and M. Niu, Chem. Eng. Technol. 441 (2022) 135942.
17. M. Heidari, M. Tahmasebpoor, and A. Antzaras, Process Saf. Environ. 144 (2020) 349-365.
18. J. Wang, M. Li, and P. Lu, Chem. Eng. J. 392 (2020) 123752.
19. V.A. Tuan and C.H. Lee, Vietnam J. Chem. 56[2] (2018) 197-202.
20. K. Ho, S. Jin, M. Zhong, A.T. Vu, and C.H. Lee, Chem. Phy. 198 (2017) 154-161.
21. K.K. Han, Y. Zhou, W.G. Lin, and J.H. Zhu, Microporous Mesoporous Mater. 169 (2013) 112-119.
22. K.K. Han, Y. Zhou, Y. Chun, and J.H. Zhu, J. Hazard. Mater. 203 (2012) 341-347.
23. H. Yu, X. Wang, Z. Shu, M. Fujii, and C. Song, Front. Chem. Sci. Eng. 12[1] (2018) 83-93.
24. S. Jin, K. Ho, and C.-H. Lee, Chem. Eng. J. 334 (2018) 1605-1613.
25. M. Lashanizadegan, F. Mousavi, and H. Mirzazadeh, J. Ceram. Process. Res. 17 (2016) 586-590.
26. Y. Lim, S. Kang, and K. Kim, J. Ceram. Process. Res. 25 (2024) 673-682.